Available online at www.sciencedirect.com
ScienceDirect
International Journal of Heat and Mass Transfer 50 (2007) 1577–1591
International Journal of HEAT and MASS TRANSFER
www.elsevier.com/locate/ijhmt

Nucleate boiling heat transfer from a structured surface – Effect of liquid intake

A.K. Das, P.K. Das *, S. Bhattacharyya, P. Saha

Department of Mechanical Engineering, Indian Institute of Technology, Kharagpur 721 302, India

Received 22 July 2005; received in revised form 16 August 2006
Available online 30 October 2006

Abstract

A model of the suction evaporation mode in nucleate boiling from tunnel and pore structures is presented. The model is based on the analysis by Nakayama et al. [W. Nakayama, T. Daikoku, H. Kuwahara, T. Nakajima, Dynamic model of enhanced boiling heat transfer on porous surfaces – Part II. Analytical model, ASME J. Heat Transfer 102 (3) (1980) 451–456] and L.H. Chein and R.L. Webb [A nucleate boiling model for structured enhanced surfaces, Int. J. Heat Mass Transfer 41 (14) (1998) 2183–2195]. Additionally, a detailed phenomenological model of liquid refill has been developed. It has been shown that the process of liquid refill and the time needed for it is strongly dependent on pool height. Effect of liquid pool height on bubble frequency has also been discussed. Finally, a generalized methodology is given for the prediction of boiling data from a structured surface.

Keywords: Heat flux; Intake time; Bubble growth; Pool height; Structured surface

1. Introduction

Maximization of heat transfer for a given volume of heat exchanger or for a given temperature difference between the fluid streams is a challenge continuously faced in the heat exchanger industry. Invention of a host of techniques for the enhancement of heat transfer is an outcome of this. Over the years researchers have studied various fundamental as well as practical aspects of the enhancement techniques covering both single-phase convection as well as heat transfer with phase change (boiling and condensation). In general, the mechanism of heat transfer augmentation is not identical in case of single-phase convection and condensation or boiling. For example in condensation, the surface is designed to either promote drop wise condensation or to improve the drainage of the accumulated condensate film. On the other hand, for nucleate boiling, the goal is to achieve higher rate of vapor generation and its removal from the heating surface.

The effect of nucleation sites on the rate of heat transfer in nucleate boiling was understood as early as 1931 by Jacob [1]. He reported enhancement of boiling heat transfer from a sand blasted surface and a surface with machined grooves. The later showed a dramatic increase in the rate of heat transfer with a reduced aging effect. This paved the path for developing various techniques for augmenting nucleate boiling heat transfer. The techniques tried for several decades can be broadly classified as active and passive. Though active techniques like surface vibration, jet impingement and EHD have shown convincing enhancement in nucleate boiling, passive techniques received wide acceptance from the industry for its inherent safety, simple design and ease of operation. Passive augmentation in nucleate boiling is obtained primarily by providing specially designed micro-structures on the surface. Industrial research has made commercial production of such surfaces possible. Time to time there has been efforts to summarize and consolidate the information and understanding regarding enhancement of nucleate boiling [2–4].

* Corresponding author. Tel.: +91 032 22282916; fax: +91 032 22282278.
E-mail address: pkd@mech.iitkgp.ernet.in (P.K. Das).

0017-9310/$ - see front matter © 2006 Elsevier Ltd. All rights reserved.
doi:10.1016/j.ijheatmasstransfer.2006.08.030

Nomenclature

A	surface area (m^2)
B	bond number
c	empirical constant in external heat flux
C_3	empirical constant for Eq. (42)
C_{pl}	heat capacity (kJ $(kg\ K)^{-1}$)
C_b	empirical constant of bubble departure diameter
C_{t1}	empirical constant for preparatory period
C_{t2}	empirical constant for Eq. (39)
C_v	coefficient of velocity
d_b	bubble departure diameter (m)
d_p	pore diameter (m)
f	bubble frequency
g	acceleration due to gravity ($m\ s^{-2}$)
h	heat transfer coefficient ($W\ (m^2\ K)^{-1}$)
h_l	height of the pool above the surface (m)
h_{fg}	latent heat ($J\ kg^{-1}$)
H_t	tunnel height (m)
Ja	Jacob number
k_l	thermal conductivity ($W\ (m\ K)^{-1}$)
k_c	empirical constant in Eq. (22)
L	tunnel length (m)
m_{in}	mass evaporated in refill stage (kg/s)
m_{l1}	mass evaporated in preparatory stage (kg/s)
m_{l2}	mass evaporated in growth stage (kg/s)
m	mass evaporated in bubble growth stage (kg/s)
m	slope of P_s vs. T_s
n_s	nucleation site density (m^{-2})
N	number of active pores
P	pressure (Pa)
P_{amb}	ambient pressure (Pa)
P_{br}	break through pressure (Pa)
P_{oe}	outside pressure of the tunnel at the intake phase (Pa)
P_p	pore pitch (m)
P_r	liquid Prandtl number
P_s	saturated pressure of liquid (Pa)
P_t	tunnel pitch (m)
P_v	vapour pressure (Pa)
P_{v2}	vapour pressure at the intake phase (Pa)
P_{v2b}	initial vapour pressure at the beginning of intake phase (Pa)
q_{evl}	heat required for evaporation of extra liquid intake (W)
q''	heat flux ($W\ m^{-2}$)
$q''_{ex.MR}$	external heat flux calculated by Mikic and Rohsenow ($W\ m^{-2}$)
q''_{ex}	external heat flux ($W\ m^{-2}$)
q''_{tun}	tunnel heat flux ($W\ m^{-2}$)
r	instantaneous radius of the bubble (m)
r_c	radius of curvature of the sloshed liquid (m)
r_{mi}	initial meniscus radius (m)
r_{mg}	meniscus radius at the beginning of the growth cycle (m)
r_{me}	meniscus radius at the end of the growth cycle (m)
r_{ne}	non-evaporating meniscus radius (m)
r_b	tunnel base radius (m)
R	universal gas constant ($kJ\ kg^{-1}\ K^{-1}$)
t	time (s)
t_i	liquid intake time through active pores (s)
t_{ii}	liquid intake time through inactive pores (s)
t_{in}	liquid intake time (s)
t'_{in}	liquid refill time (s)
t''_{in}	depressurization time (s)
t_g	bubble growth period (s)
t^*_g	non-dimensional bubble growth period
t_w	preparatory period (s)
T	temperature (K)
T_{inf}	liquid pool temperature (K)
T_s	saturation temperature (K)
T_v	vapour temperature (K)
T_{v1}	vapour temperature at the end of preparatory phase (K)
T_{v2}	vapour temperature at the end of bubble growth phase (K)
T_w	wall temperature (K)
T^r_w	reference wall temperature (K)
v_b	upward velocity of the vapor phase ($m\ s^{-1}$)
v_g	gas velocity at the moment of bubble departure ($m\ s^{-1}$)
v_{in}	velocity of liquid in the intake period ($m\ s^{-1}$)
v_l	liquid velocity for the refill stage ($m\ s^{-1}$)
V_b	bubble volume (m^3)
V_c	volume of the tunnel cavity (m^3)
V_{in}	volume of liquid intake from inactive pore (m^3)
V_{v1}	volume of vapour at the end of preparatory period (m^3)
V_{vm}	average volume of vapour at the preparatory period (m^3)
V_t	tunnel volume (m^3)
W_t	tunnel width (m)
Z_g	coordinate perpendicular to the tunnel diameter (m)

Greek symbols

α_l	liquid thermal diffusivity ($m^2\ s^{-1}$)
β	ratio of active nucleation site and total pores
ε_c	void fraction of the tunnel cavity
η_d	non-dimensional distance between bubble top and the outer surface at the active pore
ξ	non-dimensional distance between bubble top and the outer surface at the inactive pore
ΔT_{t1}	average temperature difference in the preparatory stage (K)
ΔT_{t2}	average temperature difference in the bubble-growing stage (K)

ΔT_{ws}	degree of superheat of the tunnel wall (K)
θ	contact angle
v	thermal diffusivity ($m^2 s^{-1}$)
ρ	density ($kg m^{-3}$)
ρ_l	liquid density ($kg m^{-3}$)
ρ_v	vapour density ($kg m^{-3}$)
ρ_{v1}	vapour density at the end of preparatory phase ($kg m^{-3}$)
ρ_{v2}	vapour density at the end of bubble-growing phase ($kg m^{-3}$)
ρ_{vm1}	average vapour density in the preparatory phase ($kg m^{-3}$)
ρ_{vm2}	average vapour density in the bubble-growing phase ($kg m^{-3}$)
φ^*	ratio of vapor generation rate and number of pores
σ	surface tension ($N m^{-1}$)

In a recent review Webb [5] has provided a meticulous account of enhanced boiling surfaces.

Various observations gave a prima-facie proof that the increase in the number of nucleation sites gives higher rate of heat transfer in nucleate boiling. Different manufacturing techniques were adopted to develop surfaces having a high nucleation site density. Apart from different micro-machining techniques two unique surface fabrication methods need special mention. There are surfaces made of composite material [6,7] and surface with micro-porous coating [8,9]. For instance, impregnation of graphite surface in a copper matrix [6] gives substantial rise in the boiling heat transfer. On the other hand micro-porous coating [8] provides significantly higher active nucleation site density. It increases the bubble frequency but reduces the bubble diameter and at high heat flux it reduces the superheated liquid layer thickness. Further it also delays Critical heat flux. Efforts have also been made to enhance the boiling heat transfer by modifying the bubble release pattern from the heated surface. In these methods instead of modifying the heated surface, additional structures are added slightly away from it. These include confinement in the form of perforated plates, slitted plates [10] as well as wire mesh [11,12]. In general the bubble coalescence and bubble departure can be modified to enhance the rate of heat transfer using a judicial design of such confinement devices.

It has been recognized [13] that the diameter of an artificial nucleation site determines the minimum degree of wall superheat required and its shape determines the mobility of the vapour liquid interface. A re-entrant cavity acts as a very stable vapour trap and can support the nucleation process continuously by providing a negative curvature to the bubble. Arshad and Thome [14], Nakayama et al. [15] and Xin and Chao [16] confirmed it after studying the reentrant cavities. It has been found that grooved cavities with sub-surface communication can provide further enhancement to nucleate boiling compared to isolated reentrant cavities. Accordingly, different designs have been evolved for surfaces with simple and reentrant channels for both plane and tubular surface [17]. Out of different micro-structures of re-entrant cavities the "tunnel and pore" design is one of the most effective. A description of the "tunnel and pore" structure along with schematic diagram is given later.

The difficulties of modeling a complex transport phenomenon like nucleate boiling need not be exaggerated. A recent review [18] shows that even enough experimental data are not available to quantify the effect of the thermo physical properties of the surface material (thermal conductivity and thermal absorption), interaction between the solid surface, liquid and vapor, surface micro-geometry (dimensions and shape of cracks and pores) etc. on boiling heat transfer. Fortunately, a number of systematic studies have been made to understand the physics of the boiling process from a tunnel and pore geometry. According to visualization experiments reported by Chein and Webb [19] and Nakayama et al. [15] "suction evaporation mode" is the main mode of heat transfer in nucleate pool boiling in a tunnel and pore micro-structure. When the wall superheat is moderate, bubbles are formed from a relatively small number of pores. These pores are called active pores and others are called inactive pores. The inactive pores play the vital role of supplying liquid needed for uninterrupted vapour generation through the active pores. The formation of vapour inside the tunnel, the generation of bubble at the active pores, its growth and departure involves certain complex processes which occur in a cyclic manner. Hsu and Graham [20] first proposed that bubble cycle can be divided into bubble initiation, growth and departure. With the increase of degree of superheat, pressure inside the vapour tunnels increases and after some time vapour protrudes through the pores. Then the inertia force of the liquid and the vapour generated inside the tunnel controls bubble growth up to its departure.

Nakayama et al. [21] made the pioneering effort to make a systematic analysis on the mechanism of suction evaporation mode of nucleate boiling. The basic assumption of their model is that vapour is primarily generated from the liquid menisci present at the corners of the tunnels. Pressure build-up stage, pressure reduction stage and liquid intake phase describes the total phenomena of the boiling cycle according to the model. Temporal variation of liquid meniscus thickness is ignored in their model. Nakayama et al. [21] further suggested that the total heat flux is the contribution of both tunnel heat flux and external heat flux:

$$q'' = q''_{tun} + q''_{ex} \tag{1}$$

Chein and Webb [22] proposed some modifications over the Nakayama et al. model [21] based on the suction evaporation mode of nucleate boiling. Their model needs only two empirical constants in contrast to seven in the Nakayama et al. [21] model. They have also used Eq. (1) for determining the total heat flux.

Ramaswami et al. [23] proposed some modification for the basic Nakayama et al. model [21] by suggesting a different methodology for calculating external heat flux.

Jiang et al. [24] provided a different analysis for the evaporation of the liquid meniscus. Taking a lead from the evaporation analysis in the micro-grooves on the heat pipe [25] they estimated the evaporation inside the tunnel.

The above discussion shows all the models for nucleate boiling from a tunnel and pore structures are based on the proposition of suction evaporation mode by Nakayama et al. [21]. However, the models met with varying success while correlating the experimental data. For instance Nakayama et al. [21] model does not give a good prediction of bubble frequency. Bubble frequency is predicted reasonably well by Chein and Webb [22] model. However, their heat flux prediction lies within ±33% of the experimental results [22]. Ramaswamy et al. [23] model predicts their own data within ±40%. Jiang et al. [24] predicted experimental data very well only for some special tunnel dimensions.

It is accepted that suction evaporation mode describes the process of nucleate boiling in a tunnel and pore geometry; however, its partial success in calculating the experimental data leaves a scope of reexamination of the model. It is probable that some of the physical processes during suction evaporation mode have not been considered rigorously in the earlier models. None of the earlier models made a thorough analysis of the liquid intake phase assuming it to be too brief to affect the total period of a bubble cycle. Though, this assumption is valid for a large number of situations it needs to be incorporated for the completeness of the model. Further, this is expected to improve the model prediction in limiting cases where the time taken for liquid intake is also significant in the life cycle of a bubble in the tunnel and pore geometry.

The present work revisits the suction evaporation mode of boiling in a structured surface. Taking a lead from both the Nakayama et al. [21] model and Chein and Webb [22] model the boiling heat flux is predicted. A thorough analysis of the liquid intake phase has been made. Model prediction has been compared with published experimental results and the results of earlier models.

2. Physical model

Fig. 1 schematically depicts a typical tunnel and pore structure of the sub-surface of an enhanced boiling surface. The depicted configuration consists of a straight "one-dimensional" rectangular tunnel of uniform cross-section with a series of equally spaced pores at its top surface. This is one of the widely used designs of a reentrant nucleation cavity. The tunnel structure supplies vapour from a larger sub-surface area to any active pore. It also ensures continuous replenishment of liquid needed for evaporation. It is assumed that the tunnel is sufficiently long and there are large numbers of pores so that the end effect can be neglected and the analysis can be done considering a single active pore and the associated length of the tunnel. As the phenomenon of boiling consists of many complex and inter-related processes, following idealizations are made for building a mechanistic model:

1. There are liquid menisci at the corners of the vapour filled tunnels. This gives rise to suction evaporation mode of boiling [15]. Liquid menisci and tunnel cross-section are shown in Fig. 1.

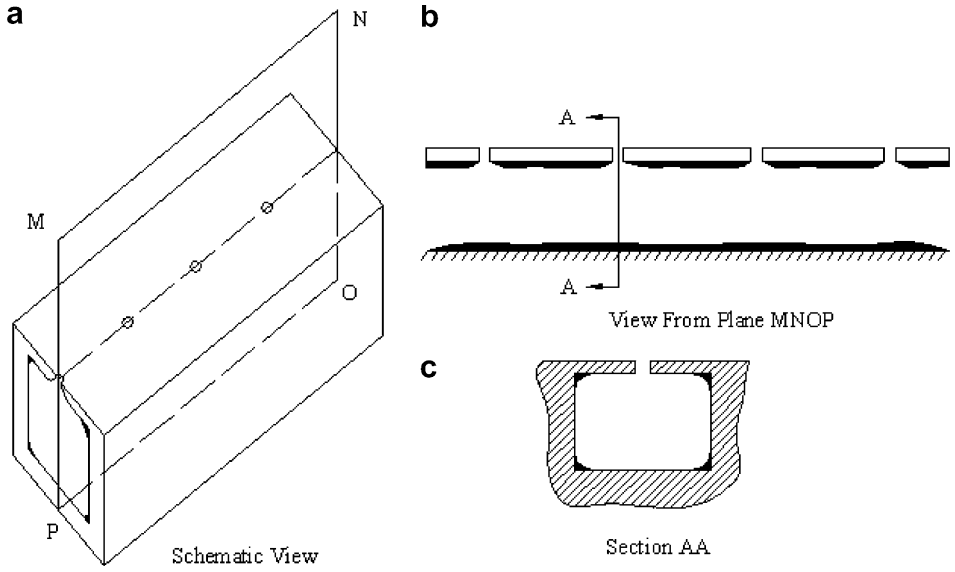

Fig. 1. Geometrical details of the boiling surface.

2. Liquid menisci are uniformly distributed along the tunnel and have the same radius of curvature throughout the tunnel length.
3. Temporal and spatial variation of the tunnel temperature is neglected.
4. Evaporation of the micro-layers above the sub-surface tunnel is neglected. Evaporation of menisci inside the tunnel is considered to be the primary mode of heat transfer.
5. One-dimensional heat conduction is employed to predict the evaporation rate.
6. Volume of liquid outside the tunnel is very large compared to the cavity size.
7. The thickness of the upper wall of the cavity is much smaller compared to its other dimensions.

Other assumptions will be stated wherever appropriate.

The process of nucleate boiling comprises of bubble formation, its growth and departure. Each of these processes is highly transient. However, one can identify a repetitive pattern in the occurrence of the above phenomena under steady operating conditions. Three mutually separable phases namely (i) preparatory phase (ii) bubble growth phase (iii) intake phase can be distinguished during boiling from a structured surface. These phases (Fig. 2a) are characterized by the typical variation of pressure inside the tunnel. An understanding of these phases is required for the development of any mechanistic model.

2.1. Preparatory phase

The process necessary to start a new bubble cycle constitutes the preparatory phase. The liquid menisci that exist in the four corners of the tunnels (shown in Fig. 1) evaporate due to direct contact with the heat source. A minimum thickness of liquid, called non-evaporating thickness, always remains at the wall of the tunnel. At this instant the pressure increases and horizontal vapour columns inside the tunnels get elongated compensating the radius of curvature of the menisci. Hence, the radius of the menisci decreases from r_{mi} to r_{mg} as shown in Fig. 2a. This phenomenon occurs till the pressure inside the tunnel becomes equal to the breakthrough pressure of the pore. At the same time the diameter of the extruded bubble becomes equal to the diameter of the pore. This breakthrough pressure is a function of surface tension of the tunnel–liquid combination and the pore diameter ($P_{br} = 4\sigma/d_p$). When the pressure inside the tunnel exceeds the break through pressure (P_{br}) the bubble starts to blossom outside the pore.

2.2. Bubble growth phase

In this phase the bubbles are pushed due to continuous vapour generation inside the tunnel. The vapour phase is extruded outside the pore with some inertia for the pressure difference between the liquid pool and the interior of the tunnel. As a result the bubble dimension increases. However, at initial phase of bubble growth one can observe an oscillatory nature of the vapour liquid interface. Probably some of the vapour mass which comes out of the tunnel bounces back to it resulting in a temporal decrease of the bubble volume. Over a period the bubble increases in volume and once the centre of the bubble comes out of the pore the bubble continues to grow till it departs from the surface. This has been observed at low degree of superheat.

During the growth phase the liquid menisci radius inside the tunnel changes from r_{mg} to r_{me}. Nevertheless, r_{me} never supersedes the limiting radius r_{ne} which is given by

$$r_{ne} = \frac{\sigma}{\Delta T_{ws}}\left(\frac{dT}{dP}\right) \tag{2}$$

Void fraction of the cavity decreases continuously compared to the preparatory phase due to the rapid evaporation of the meniscus. The bubbles continuously increase

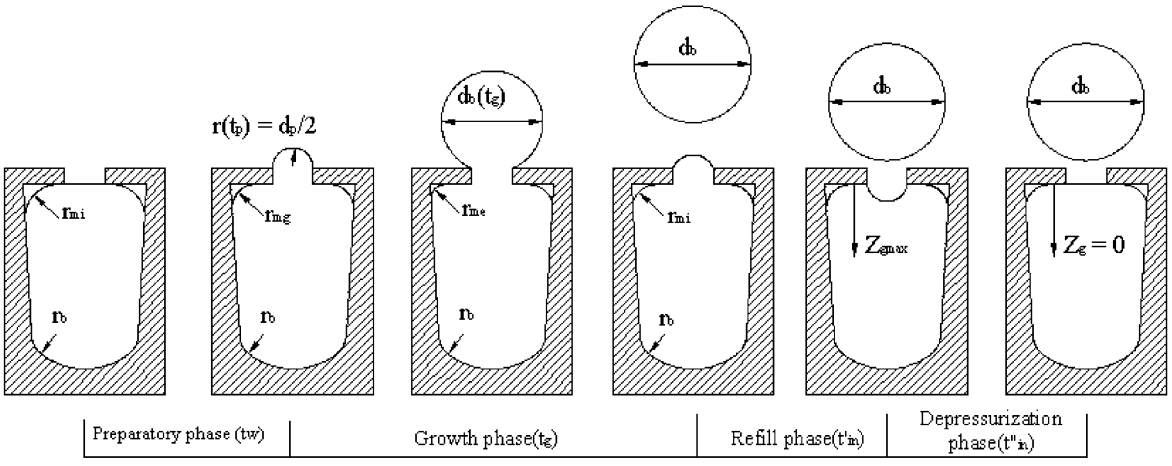

Fig. 2a. Stages of a bubble cycle from a structured surface.

in size after the initial instability in dimension. At the end of this period the bubbles have diameter d_b termed as departure diameter.

2.3. Liquid intake phase

After the bubble departure, the ambient liquid pressure is usually lower than the cavity pressure for a small pool height. So the liquid cannot enter through the active pores overcoming the excess pressure. To continue the suction evaporation mode and to compensate for the liquid evaporated during bubble departure, liquid enters the tunnel through inactive pores. This entry of liquid takes a very small time compared to the other two phases. Number of active pores increases with the degree of superheat. So increase in degree of superheat cuts the liquid supply line decreasing the number of inactive pore. When the pool liquid height increases the liquid intake time decreases and after a certain pool height liquid also tend to penetrate through the vapour menisci present at the active pores. However, the process of liquid intake through the active pores is different from that through the inactive pores. While in the former a liquid finger protrudes in a vapour filled space, in the later it enters in a flooded cavity. It may further be assumed that the liquid intake processes for the active and inactive pores are independent of each other. We suggest a phenomenological model for the liquid penetration through the active pores. It may be divided into two phases namely, liquid refill stage and depressurization stage.

2.3.1. Liquid refill stage

At the instant a bubble detaches from a pore, the vapour pressure is higher than the pressure of the surrounding liquid. But just after the bubble departure the tunnel pressure suddenly decreases and a liquid sloshing into the tunnel occurs. This can be defined as liquid refill stage. The intake continues till the pressure of the cavity equals the outer pool or the intake velocity becomes identical to the upward velocity of the vapour phase (v_b). During this process some extra amount of liquid gets into the cavity over and above the liquid evaporated in the previous cycle. As a result the liquid vapour interface becomes concave downward.

2.3.2. Pressurization stage

To start the preparatory phase again, the pressure inside the cavity must increase. During this phase the curvature of the interface becomes infinity due to the increase of the pressure inside the cavity. But in general pressure difference between the pool and tunnel is so small that liquid intake time is negligible in comparison to the other two stages. However, for an accurate prediction of the heat flux it is not wise to neglect it. At the end of the liquid intake phase the menisci radius again becomes r_{mi} which denotes the initiation of the next cycle.

Throughout the bubble cycle void fraction is maintained by the intake of liquid through the inactive pores for a fixed degree of superheat. The liquid entering through the active pores do not contribute substantially to the tunnel liquid inventory. However, the protrusion of the liquid finger through the active pores just after the departure of a bubble and its subsequent expulsion due to the increase of vapour pressure take some finite amount of time. This needs to be considered in the estimation of total cycle time.

3. Mathematical formulation

3.1. Time needed for preparatory phase

Considering the effect of inertia and heat diffusion Mikic and Rohsenow [26] derived an expression for the rate of bubble growth

$$r(t)=2\sqrt{\frac{3}{\pi}}Ja\sqrt{\alpha_l t}\left\{1-\frac{(T_w-T_{inf})}{(T_w-T_s)}\left[\left(1+\frac{t_w}{t}\right)^{1/2}-\left(\frac{t_w}{t}\right)^{1/2}\right]\right\} \tag{3}$$

Now at $t=t_g$, $r(t)=d_b/2$, and hence

$$\frac{d_b}{2}=2\sqrt{\frac{3}{\pi}}Ja\sqrt{\alpha_l}\left\{\sqrt{t_g}-\frac{(T_w-T_{inf})}{(T_w-T_s)}\left[(t_g+t_w)^{1/2}-(t_w)^{1/2}\right]\right\} \tag{4}$$

Simplifying Eq. (4) we obtain

$$t_w=\left(\frac{t_g Q}{2P}-\frac{P'}{2Q}\right)^2 \tag{5}$$

where $P'=\frac{d_b}{4\sqrt{\frac{3}{\pi}}Ja\sqrt{\alpha_l}}-\sqrt{t_g}$ and $Q=\frac{(T_{inf}-T_w)}{(T_w-T_s)}$.

Waiting period depends on bubble departure diameter and bubble growth time (t_g) which will be evaluated in the later sections.

3.2. Estimation of bubble departure diameter

By balancing the buoyancy force and the surface tension force of a growing bubble Nakayama et al. [21] developed an empirical relation for d_b based on physical parameters.

They neglected the inertia force of the vapour bubble to yield

$$d_b=c_b\left[\frac{2\sigma}{(\rho_l-\rho_{vm2})g}\right]^{1/2} \tag{6}$$

Experimental data of Nakayama et al. [15] showed that c_b for R-11 is 0.42 and for water it is 0.22. Haider [27] established an expression for c_b as a function of the contact angle θ:

$$c_b=(3\sin\theta)^{1/3}\left(\frac{2\sigma}{(\rho_l-\rho_v)g}\right)^{-1/6} \tag{7}$$

where $\theta=\sin^{-1}\left(\frac{d_p}{d_b}\right)$.

Now the bubble departure diameter can be calculated for a specific liquid–solid combination.

3.3. Calculation of bubble growth time

Chein and Webb [22] suggested that growth of a bubble on a structured surface is different from plane surface. In case of a structured surface vapour is supplied only from the tunnels. Depending on the vapour pressure and surface tension force Mikic and Rohsenow [28] have derived the bubble growth rate as

$$\left(\frac{\mathrm{d}r}{\mathrm{d}t}\right)=\left[\left(\frac{\pi}{7}\frac{h_{\mathrm{fg}}\rho_{\mathrm{v}}\Delta T_{\mathrm{ws}}}{\rho_{\mathrm{l}}T_{\mathrm{s}}}\right)\left(\frac{T_{\mathrm{v}}-T_{\mathrm{s}}}{T_{\mathrm{w}}-T_{\mathrm{s}}}\right)\right]^{1/2} \tag{8}$$

Chein and Webb [22] suggested that, at $t=0$, bubble radius $(r)=d_{\mathrm{p}}/2$ and at $t=t_{\mathrm{g}}$, bubble radius $(r)=d_{\mathrm{b}}/2$.

Eq. (8) can be readily integrated to estimate the growth time t_{g}:

$$t_{\mathrm{g}}=33.784\left[\frac{7}{\pi}\frac{\rho_{\mathrm{l}}T_{\mathrm{s}}}{h_{\mathrm{fg}}\rho_{\mathrm{v}}\Delta T_{\mathrm{ws}}}\frac{(d_{\mathrm{b}}+d_{\mathrm{p}})}{(d_{\mathrm{b}}-d_{\mathrm{p}})}\right]^{1/2}\left(\frac{d_{\mathrm{b}}-d_{\mathrm{p}}}{2}\right) \tag{9}$$

Once t_{g} and d_{b} are known t_{w} can be calculated from Eq. (5).

3.4. Determination of important physical properties

At the beginning of the bubble cycle let the pressure, density and temperature of the vapour phase be donated by P_{v}, ρ_{v}, T_{v}, respectively.

Combining Clausius–Clapeyron relation:

$$\frac{\mathrm{d}T_{\mathrm{v}}}{\mathrm{d}P_{\mathrm{v}}}=\frac{T_{\mathrm{v}}}{\rho_{\mathrm{v}}h_{\mathrm{fg}}} \tag{10}$$

and equation of state:

$$P_{\mathrm{v}}=\rho_{\mathrm{v}}RT_{\mathrm{v}} \tag{11}$$

yields

$$T_{\mathrm{v1}}=T_{\mathrm{v}}+\left(\frac{4\sigma}{d_{\mathrm{p}}}\right)\frac{T_{\mathrm{v}}}{\rho_{\mathrm{v}}}h_{\mathrm{fg}} \tag{12}$$

and

$$\rho_{\mathrm{v1}}=\rho_{\mathrm{v}}+\left(\frac{4\sigma}{d_{\mathrm{p}}}\right)\frac{\left(1-\frac{RT_{\mathrm{v}}}{h_{\mathrm{fg}}}\right)}{RT_{\mathrm{v}}} \tag{13}$$

Then one can estimate the average density during preparatory phase and growth phase:

$$\rho_{\mathrm{vm1}}=(\rho_{\mathrm{v}}+\rho_{\mathrm{v1}})/2 \tag{14}$$

$$\rho_{\mathrm{vm2}}=(\rho_{\mathrm{v1}}+\rho_{\mathrm{v2}})/2 \tag{15}$$

where

$$\rho_{\mathrm{v2}}=\rho_{\mathrm{v}}+\left(\frac{4\sigma}{d_{\mathrm{b}}}\right)\frac{\left(1-\frac{RT_{\mathrm{v}}}{h_{\mathrm{fg}}}\right)}{RT_{\mathrm{v}}} \tag{16}$$

and ρ_{vm2} is related to bubble departure diameter by the following equation:

$$d_{\mathrm{b}}=c_{\mathrm{b}}\sqrt{\frac{2\sigma}{(\rho_{\mathrm{l}}-\rho_{\mathrm{vm2}})g}} \tag{17}$$

From Eqs. (14)–(17) we get

$$\rho_{\mathrm{vm2}}=\frac{(4Y-Z^2)+\sqrt{(Z^2-4Y)^2-16(Z^2\rho_{\mathrm{l}}-Y^2)}}{8} \tag{18}$$

where $Z=\frac{4\sigma(1-RT_{\mathrm{s}}h_{\mathrm{fg}})}{0.442RT_{\mathrm{s}}\sqrt{\frac{2\sigma}{g}}}$ and $Y=\rho_{\mathrm{vm1}}+\rho_{\mathrm{v}}$.

Vapour density at the instant of bubble departure is obtained as

$$\rho_{\mathrm{v2}}=2\rho_{\mathrm{vm2}}-\rho_{\mathrm{v1}} \tag{19}$$

The value of T_{v2} can be determined as well:

$$T_{\mathrm{v2}}=T_{\mathrm{v}}+\left(\frac{4\sigma}{d_{\mathrm{b}}}\right)\frac{T_{\mathrm{v}}}{\rho_{\mathrm{v}}h_{\mathrm{fg}}} \tag{20}$$

After determining the values of the relevant physical properties we can calculate the mass of the liquid evaporated in various stages separately. It can be seen that in bubble growth phase the amount of vapour evaporated is more than the mass evaporated in the preparatory phase.

3.5. Estimation of liquid intake time for active pores

Liquid intake through active pores occurs only for large pool heights. At larger pool height ambient pressure is greater than the pressure in the vapour tunnels below the active pores at the moment of bubble departure. As a result "gulping" of liquid occurs from the active pores that cannot be seen for smaller pool height. This phase can be defined as refill stage.

As has been mentioned earlier there is a sudden reduction of pressure when a vapour bubble leaves an active pore. Following the analysis of Tehrani et al. [29] one can apply Bernoulli's equation to find out the tunnel pressure (P_{v2b}) just after the release of bubble. This needs the knowledge about the velocity of gas at the instant of departure of the bubble. From a flooding criterion Wallis [30] relates the phenomena when gas blow down ends and liquid refill begins through an empirical relationship:

$$v_{\mathrm{g}}\left(\frac{\rho_{\mathrm{g}}}{(\rho_{\mathrm{f}}-\rho_{\mathrm{g}})gd_{\mathrm{p}}}\right)^{1/2}\leqslant 0.5 \tag{21}$$

Using Eq. (21) one gets the final expression as Eq. (22):

$$P_{\mathrm{v}_{2b}}=\rho_{\mathrm{v}_2}RT_{\mathrm{v}_2}-0.1375gd_{\mathrm{p}}(1+k_{\mathrm{c}})(\rho_{\mathrm{l}}-\rho_{\mathrm{v}_2}) \tag{22}$$

where the value of k_{c} is 0.5 as reported by Tehrani et al. [29].

At this point it is important to assess the significance of surface tension force as the process involves formation and departure of bubbles through small pores. Two different criteria has been used for this purpose. The value of Kapitsa number $Ka=(\rho^3\mathrm{g}\mathrm{v}^4/\sigma^3)^{1/6}$ in the present context is 0.0188, which is less than the critical value of 0.06. However, the capillary length $\left(\sqrt{2\sigma/\rho g}\right)$ for the fluid in interest is much too bigger compared to the pore diameter necessitating inclusion of surface tension term in the outer pressure expression. Pressure outside the cavity opening point

at the time of bubble departure depends on the height of the liquid and the surface tension due to the initial curvature of the liquid vapour interface:

$$P_{oe} = P_{amb} + \rho_l g h_l + \frac{2\sigma}{r_c} \tag{23}$$

where r_c is the curvature of the vapour liquid interface that can be defined as (Fig. 2b):

$$r_c = \frac{d_p^2 + Z_g^2}{2Z_g} \tag{24}$$

As the volume of liquid intake is very small compared to the pool liquid, P_{oe} will not vary throughout the liquid refill stage. Now the rate of pressure change can be taken as

$$\frac{dP_{v_2}}{dt} = \frac{P_{v_2} v_l (\pi d_p^2)}{4\varepsilon_c V_c} \tag{25}$$

where void fraction of the cavity can be taken as

$$\varepsilon_c = \frac{(4-\pi) r_{ne}^2}{W_t H_t} \tag{26}$$

Rate of change of liquid refill velocity can be derived from the momentum balance of the liquid outside the cavity. At the starting of liquid refill phase we assume that the velocity of the liquid phase is a sole function of pool height:

$$[\rho_l H_t - (\rho_l - \rho_{v_2}) Z_g] \frac{dv_l}{dt} = (P_{v_2} - P_{oe}) - g[\rho_l H_t - (\rho_l - \rho_{v_2}) Z_g] + \frac{\rho_{v_2} v_l^2 Z_g A}{\varepsilon_c V_c} \tag{27}$$

Depending on the velocity of the liquid phase the vapor liquid interface will start penetrating downwards through the active pores of the boiling surface as shown in Fig. 2b. We define Z_g as the maximum depth of the interface below the pore mouth. Rate of change of Z_g gives the liquid velocity:

$$\frac{dZ_g}{dt} = v_l \tag{28}$$

The initial boundary conditions are taken as
At $t_{in} = 0$, $Z_g = 0$, $v_l = C_v\sqrt{2gh_l}$, $P_{v2} = P_{v2b}$.

When the pressure inside the cavity equals the outside pressure, the liquid refill stage ends. Moreover if the liquid refill velocity becomes greater than the upward velocity of the vapour phase, the intake of liquid also stops and bubble formation starts.

In this liquid refill stage total amount of liquid refill can be evaluated as

$$m_{in} = \int_0^{t'_{in}} v_l \frac{\pi}{4} d_p^2 \, dt \tag{29}$$

Amount of liquid to be filled to make the continuity for next stage is $\frac{\pi d_b^3 \rho_{v_2}}{6\rho_l}$.

Then the extra amount of liquid that is taken in the liquid refill stage, have to be expelled in the next stage from the cavity. During this pressure inside the cavity also increases to some extent to start the preparatory phase again.

Total heat required to evaporate the extra liquid intake inside the cavity is

$$q_{evl} = \rho_l \left[\int_0^{t'_{in}} v_l \frac{\pi}{4} d_p^2 \, dt - \frac{\pi d_b^3 \rho_{v_2}}{6\rho_l} \right] h_{fg} \tag{30}$$

The time required to gain this amount of energy from the tunnel wall is defined as t''_{in}. It can be evaluated as

$$t''_{in} = \frac{\rho_l}{q''_{tun} L (2H_t + W_t)} \left[\int_0^{t'_{in}} v_l \frac{\pi}{4} d_p^2 \, dt - \frac{\pi d_b^3 \rho_{v_2}}{6\rho_l} \right] h_{fg} \tag{31}$$

It needs an iteration process to calculate tunnel heat flux and pressurization time using the liquid refill time from active pores.

3.6. Calculation of liquid intake time from inactive pores

Liquid enters from the inactive pores to maintain certain void fraction. This entry is completely a liquid–liquid phenomenon. Volume of the liquid that is mainly involved in bubble generation (V_{in}) can be calculated from a mass balance around the pore:

$$V_{in} = \frac{\pi}{6} \frac{d_b^3 \rho_{v2}}{\rho_l} \tag{32}$$

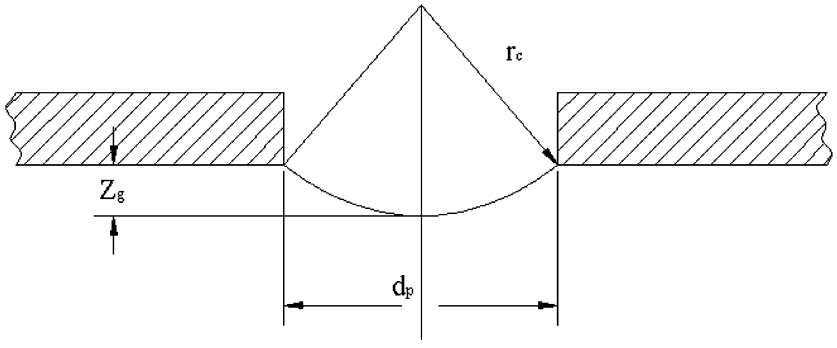

Fig. 2b. Vapour liquid interface after the bubble departure.

Initial velocity of the liquid entering through the inactive pore is a function of the liquid pool height also. Assuming the liquid of the pool to be static we can use the static pressure for calculating initial liquid intake velocity. Hence, $v_{in} = C_v\sqrt{2gh_l}$, where h_l is the pool liquid height.

Thus the liquid intake time is expressed as

$$t_{ii} = \frac{\frac{\pi}{6}d_b^3\frac{\rho_{v2}}{\rho_l}}{\frac{\pi}{4}d_p^2 C_v\sqrt{2gh_l}} \tag{33}$$

For larger pool height, liquid intake occurs simultaneously through active and inactive pores. However, the time taken for liquid intake by these two types of pores is different. The greater of them (t_i) should be considered as the liquid intake time (t_{in}) and should be used for the estimation of bubble cycle. For moderate pool height, liquid intake from active pores is absent and liquid enters the tunnel only through the inactive pores. Hence,

$$t_{in} = t_{ii} \tag{34}$$

Then we calculate the bubble frequency with the help of three individual time periods:

$$f = \frac{1}{t_w + t_g + t_{in}} \tag{35}$$

3.7. Calculation of mass evaporated in various phases

After determining the value of all the physical properties we can calculate the mass of the liquid evaporated in various stages separately. At the end of the preparatory phase the vapour volume is given by the tunnel volume and the volume of the bubbles formed on the active pores:

$$\text{At} \quad t = t_w, \quad V_{v1} = V_t + N\left(\frac{\pi d_p^3}{12}\right) \tag{36}$$

Average volume of vapour generated during the preparatory phase:

$$V_{vm} = (V_t + V_{v1})/2 \tag{37}$$

Tunnel volume for the rectangular tunnel cross-section is the product of tunnel length and cross-sectional area. Total number and pitch of the pores are N and P_p, respectively. Cross-sectional area of the rectangular tunnel is the product of tunnel height (H_t) and tunnel width (W_t). For a fixed value of V_{vm}, mass evaporated in the preparatory time effects the process of boiling in two ways. It compensates the density change due to temperature change and also feeds the growing bubble.

Hence, mass required for preparatory phase is expressed as

$$m_{l1} = V_{vm}(\rho_{v1} - \rho_v) + N\left(\frac{\pi d_p^3}{12}\right)\rho_{vm1} \tag{38}$$

Total amount of mass evaporated during growth, refill and pressurization phases can be obtained through a simple equation of energy transfer considering the durations of the respective phases:

$$m_{l2} = (t_g + t'_{in} + t''_{in})\left(\frac{k_l\Delta T_{t2}}{h_{fg}}\right)c_{t2} \tag{39}$$

where $\Delta T_{t2} = T_w - (T_{v1} + T_{v2})/2$.

Value of c_{t2} can vary for various liquid surface combinations. Nakayama et al. [21] reported a value of c_{t2} for R-11 and copper combination as 2.773×10^4 cm.

3.8. Calculation of tunnel heat flux

As all the pores are not active Nakayama et al. [21] defined a non-dimensional parameter (φ^*) to quantify the rate of vapour generation from the active pores:

$$\varphi^* = \frac{6k_l c_{t2}\Delta T_{t2}}{\rho_{vm2}h_{fg}\sqrt{2\sigma/d_p\rho_l}N\pi\frac{d_p^2}{4}} \tag{40}$$

The ratio of active pores to the total number of pores (β) is a function of t_g^*, ξ and η_d. Here t_g^* is the non-dimensional bubble growth time and it can be expressed as

$$t_g^* = \frac{t_g}{\sqrt{\frac{\rho_l d_p^3}{8\sigma}}} \tag{41}$$

ξ is assumed to be proportional to the cube root of the volume of liquid introduced during the cycle. Using an empirical constant C_3 it can be expressed as

$$\xi = -C_3[8(m_{l1} + m_{l2})/\rho_l N\pi d_p^3]^{1/3} \tag{42}$$

Value of C_3 in case of R-11 and copper combination is 3.172 [21]. η_d is the ratio to the bubble departure diameter and pore diameter:

$$\eta_d = \frac{d_b}{d_p}\left[1 + \sqrt{1 - (d_p/d_b)^2}\right] \tag{43}$$

Now β can be expressed as a function of t_g^*, ξ and η_d. Nakayama et al. [21] established an equation of β from mass conservation equation at active sites and inactive sites. Integration of the mass conservation equation from $t = 0$ to $t = t_g$ yields the following:

$$\beta = \frac{\varphi^* t_g^* - \xi(\xi^3 + 3) + 4}{\eta_d(\eta_d^3 + 3) - 4} \tag{44}$$

We can calculate the activation ratio of the pores directly from the above equation. Consequently, tunnel heat flux can be calculated directly from the energy balance of the entire cycle as shown below:

$$q''_{tun} = (m_{l1} + m_{l2})h_{fg}\beta/(t_w + t_g + t_{in})A \tag{45}$$

3.9. Calculation of external heat flux

Haider [27] and Webb [4] suggested an asymptotical solution for the external heat flux. They used Mikic and

Rohsenow [28] correlation to determine the heat transfer by transient conduction:

$$q''_{\mathrm{ex.MR}} = 2\sqrt{\pi k_{\mathrm{l}}\rho_{\mathrm{l}}c_{p\mathrm{l}}f}\,d_{\mathrm{b}}^{2}n_{\mathrm{s}}(T_{\mathrm{w}} - T_{\mathrm{s}}) \tag{46}$$

where $n_{\mathrm{s}} = \frac{q''_{\mathrm{tun}}}{\rho_{\mathrm{v}}h_{\mathrm{fg}}f\pi d_{\mathrm{b}}^{3}/12}$.

Haider [27] and Webb [4] used $q''_{\mathrm{ex.MR}}$ in their own asymptotes and found the corrected value of q''_{ex} given by

$$q''_{\mathrm{ex}} = q''_{\mathrm{ex.MR}}\left[1 + \left(\frac{0.66\pi c}{P_r^{1/6}}\right)^{2}\right]^{1/2} \tag{47}$$

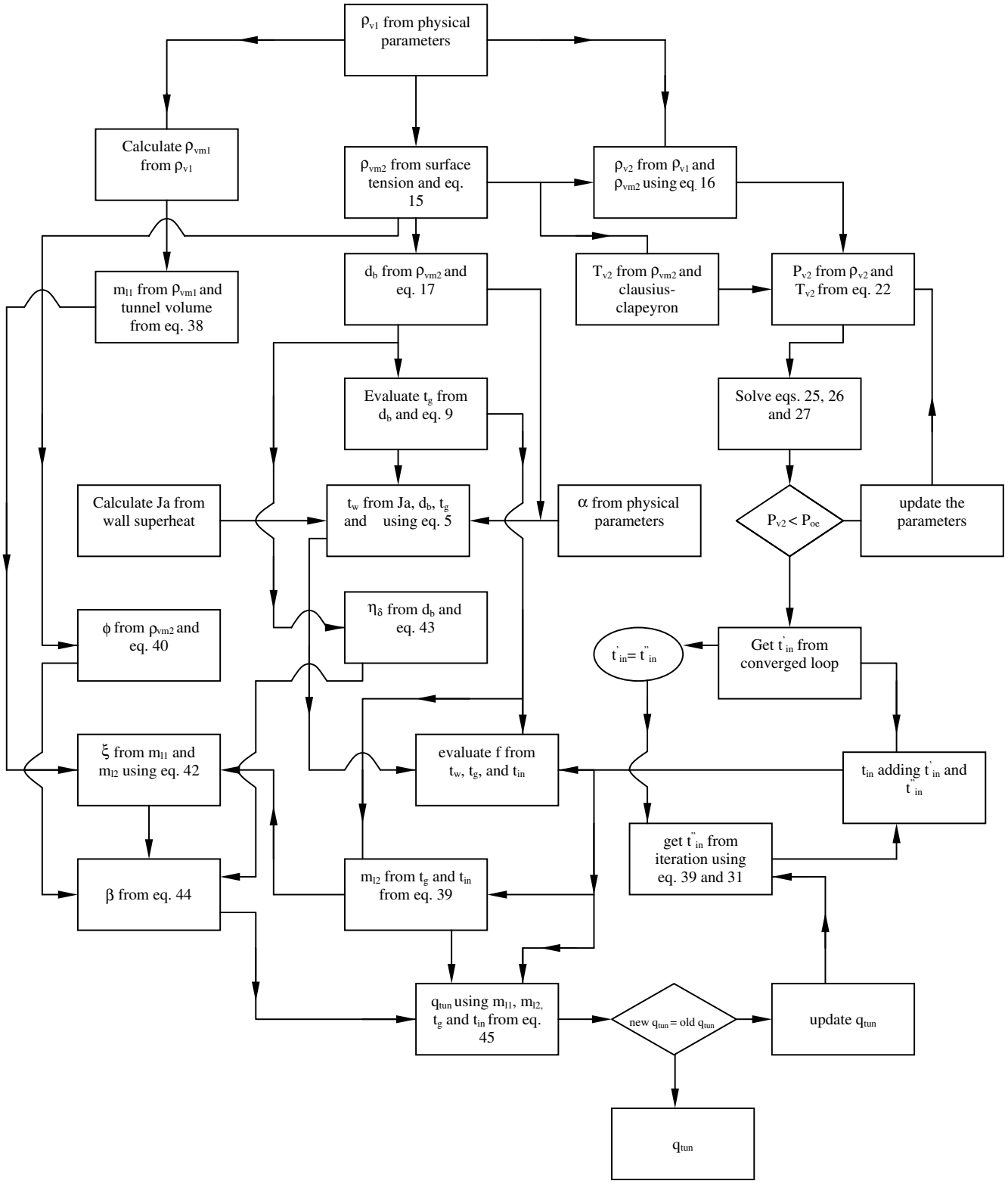

Fig. 3. Flow chart of the computational procedure.

The above expression needs the knowledge of c which is an empirical constant. Haider [27] has suggested a value of c as 6.42 by regressing the experimental data of Nakayama et al. [21] and Chein and Webb [22]. He further reported that using this empirical constant external heat flux could be predicted within an accuracy of 25% and suggested this value for any liquid–metal combination. As the external heat flux is substantially lower than the tunnel heat flux (this will be demonstrated in a later section) and as its contribution to the total heat flux is relatively small, in the present analysis Eq. (47) has been adopted with a value of $c = 6.42$.

4. Prediction procedure

The above model can predict overall heat flux (q'') for various degrees of superheat ($T_w - T_s$) for a given surface geometry (d_b, P_p, H_t, W_t), physical properties of fluid (ρ_v and T_v) and system pressure (P_v). For this a set of differential equations and algebraic equations have to be solved simultaneously. We use Runge–Kutta fourth order scheme for solving the set of differential equations (25), (27) and (28). When the outside pressure equals the tunnel pressure the solutions converges. This pressure and liquid velocity are taken as the initial conditions of the pressurization stage. A simple iteration scheme is used to calculate tunnel heat flux and liquid intake time accurately. A flow chart in Fig. 3 depicts the algorithm of the computation.

Table 1
Values of constants used for proposed models

Constants	Values
c_b	0.42
C_{bg}	0.0296
C_{t2}	2.773×10^4 cm
C_3	3.172
c	6.42
k_c	0.5

5. Results and discussion

The model has been employed to predict the heat flux for R-11, boiling on a micro-structured copper surface. The different constants used for this combination of liquid and solid are provided in Table 1. For a comparison with the predictions of other existing models simulations have also been done based on Nakayama et al. [21] and Chein and Webb [22].

It is interesting to note that time taken for the preparatory phase and the growth phase are dependent on the degree of superheat, the growth phase being more sensitive to this parameter. However, the liquid pool height does not have any effect on these two phases. On the contrary, the intake phase is independent of degree of superheat but decreases with pool height. Up to a certain pool liquid height, intake process from active pores is not possible due to the ambient pressure being lower than that of the tunnel. For atmospheric pressure acting on a pool of liquid R-11 this height is nearly 0.265 m. This is clearly evident in Fig. 4, which uses the Nakayama et al. [21] and Chein and Webb [22] model to predict the preparatory and growth

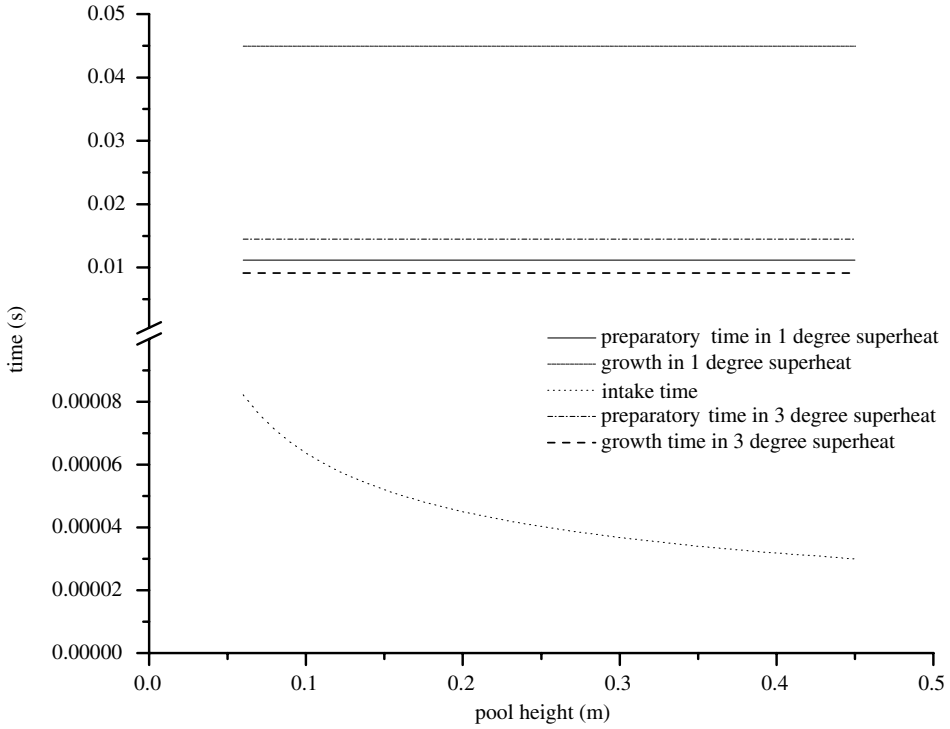

Fig. 4. Comparison of various phase spans for 1-degree superheat.

time. Intake time is evaluated for Fig. 4 by taking care of the suction evaporation mode behavior of the liquid menisci.

It can be further noted from Fig. 4 that the liquid intake time is an order of magnitude less than the time taken by the other phases. This has been assumed in the previous works without any rigorous calculation. However, omission of intake time may induce significant error for extremely low pool height, low "g" condition and systems under depressurization. With the current interest in miniaturized heat transfer equipment one needs to reexamine the applicability of the existing models. Such applications warrant a special attention on the effect of low liquid height on boiling heat transfer.

Variation of tunnel pressure and outside pressure with pool height for 1-degree superheat is shown in Fig. 5 to explore the effect of the pool height on intake. The variation of pool pressure and tunnel pressure with liquid pool height as well as degree of superheat are depicted in Fig. 5. At a low value of pool pressure liquid enters the tun-

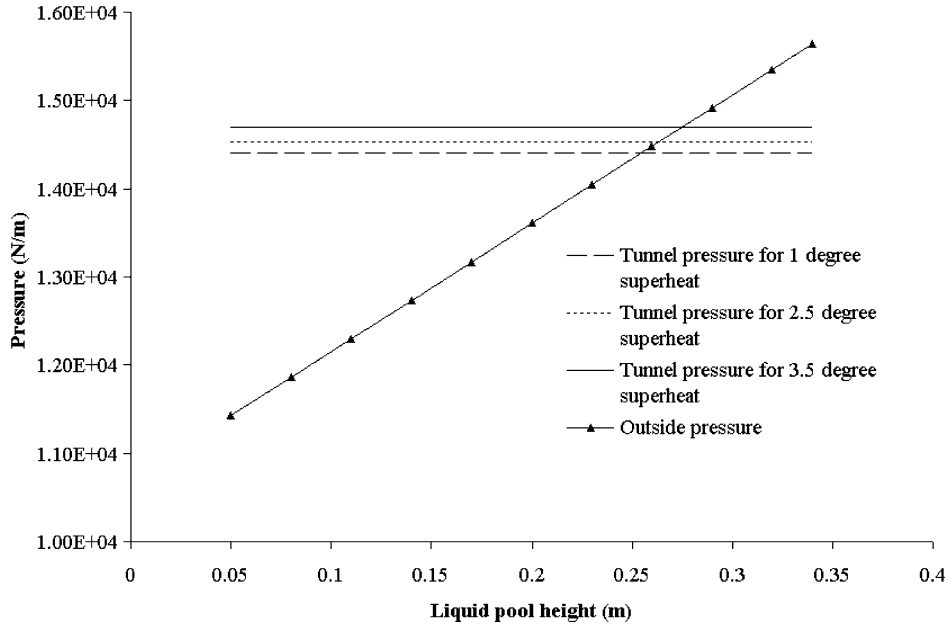

Fig. 5. Variation of tunnel pressure and outside pressure with pool height for 1-degree superheat.

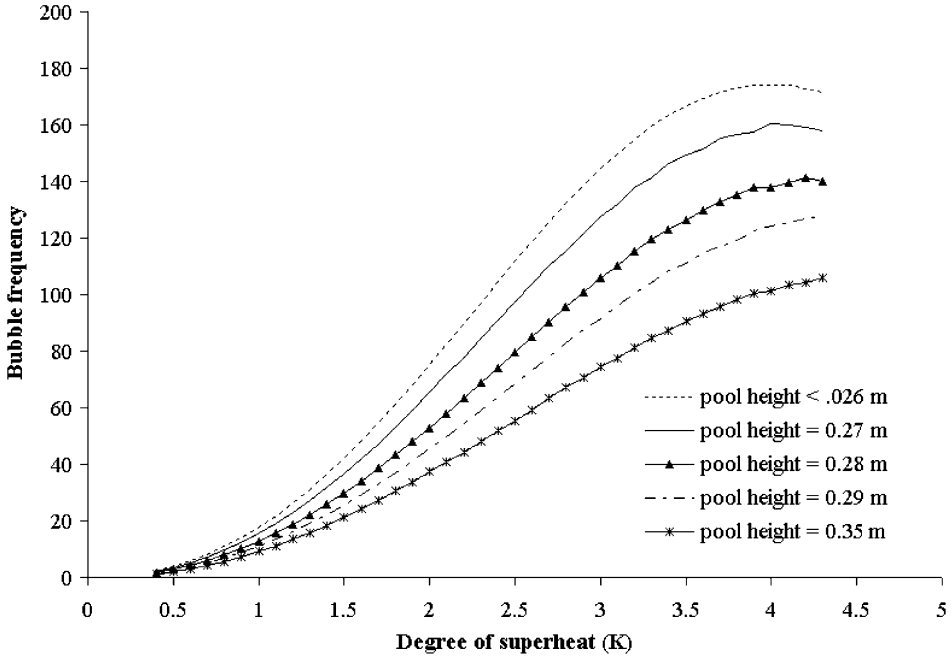

Fig. 6. Prediction of bubble frequency vs. degree of superheat for various pool heights.

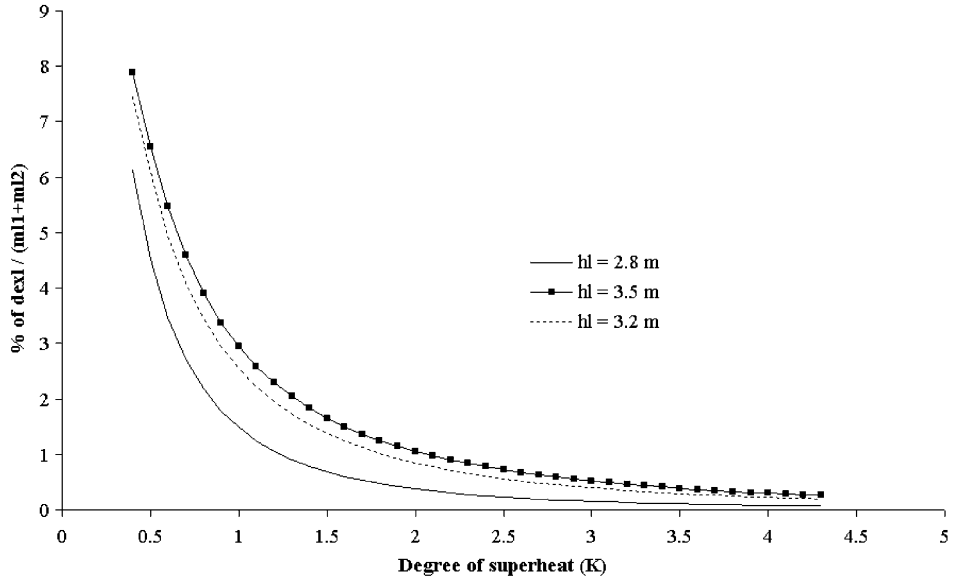

Fig. 7. Percentage of mass entered in intake phase from active pore to the total mass evaporated vs. degree of superheat.

nel only through inactive pores, whereas for comparable values of pool and tunnel pressure, liquid also penetrates through the active pores as explained earlier. While the tunnel pressure is independent of pool height and changes with the degree of superheat the outside pressure is a strong function of pool height (Eq. (23)). This implies for $P_{oe} > P_{v2}$, inclusion of liquid intake time has little impact on the heat flux from tunnel and pore geometry. However, for $P_{oe} < P_{v2}$, liquid intake time needs to be considered for an accurate prediction.

Bubble frequency decreases with pool height (Fig. 6). With the increment of pool height larger amount of excess liquid enters through the active pores and pressurization time increases resulting in a low bubble frequency. The extra mass, which enters into the cavity due to the pressure difference, as a percentage of the total mass evaporated, is shown in Fig. 7 for various pool heights. This clearly shows the effect of liquid height on the boiling process.

Bubble departure diameter is predicted well by the Haider's [27] model compared to the Nakayama et al. [21]

Table 2
Comparison of bubble departure diameter with the experimental data

Prediction	Fluid	d_p (mm)	$d_{b,exp}$ (mm) [8]	$d_{b,pred}$ (mm)
Nakayama et al. [1]	R-11 at 1 atm	0.1	0.7 ± 0.1	0.53
Proposed model	R-11 at 1 atm	0.1	0.7 ± 0.1	0.698

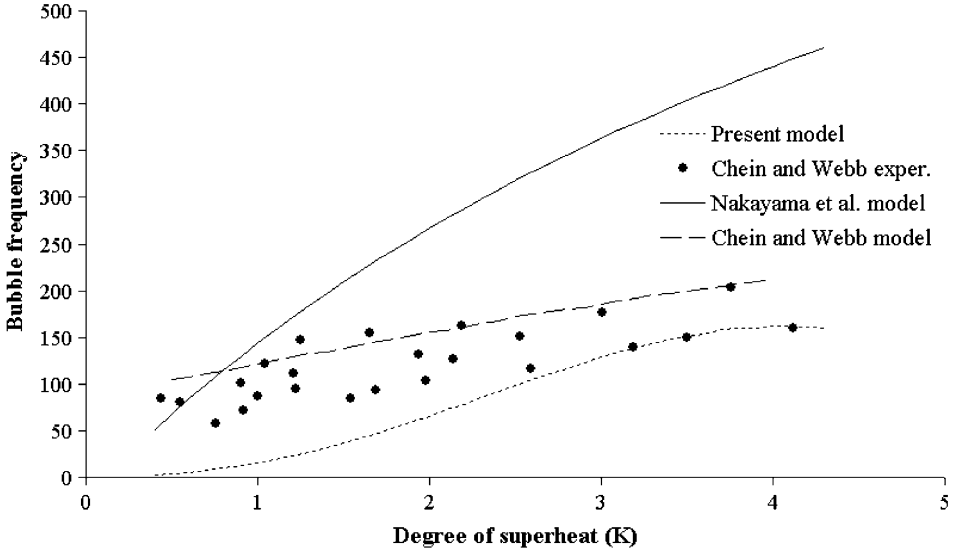

Fig. 8. Prediction of bubble frequency in proposed and previous models for pool height 0.15 m.

model. The same is used in the present simulation. For R-11 at atmospheric pressure the model prediction with the experimental result are shown in Table 2.

The prediction of the bubble frequency at moderate liquid pool height for R-11 by the present model is shown in Fig. 8. Though, the present model depicts the correct trend of bubble frequency as a function of wall superheat, the data are under predicted. On the other hand, Nakayama et al. model [21] grossly over predicts the bubble frequency data (particularly for pool heights greater than the critical pool height). Chein and Webb model [22] clearly shows a better prediction of bubble frequency in comparison with the other two models.

The main purpose of the present study is to develop a model for the prediction of total heat flux from an augmented surface having "tunnel and pore" geometry. This could be done easily using Eq. (1) by adding up q''_{tun} (Eq. (45)) and q''_{ex} (Eq. (47)). However it would be interesting to compare these two heat fluxes. This will clearly bring out the improvement obtained by adopting a structured surface. Table 3 reports the tunnel heat flux and external heat flux as a function of wall superheat for the experimental conditions reported by Nakayama et al. [15]. For the entire wall superheat range the tunnel heat flux is one order of magnitude higher compared to the external heat flux.

Table 3
Comparison of tunnel heat flux and external heat flux for various degree of superheat

Degree of superheat	Total heat flux (W/m^2)	Tunnel heat flux (W/m^2)	External heat flux (W/m^2)
1.0	1729.86	1597.13	132.73
1.5	7524.83	6901.02	623.81
2.0	20699.21	19028.6	1670.61
2.5	43872.13	40282.07	3590.06
3.0	78020.66	71545.17	6475.49
3.5	121799.56	111445.38	10354.18
4.0	171585.08	156142.37	15442.71

Finally, the data for total heat flux reported in the literatures have been compared with the Nakayama et al. [21] model, Chein and Webb model and the proposed model. Fig. 9 Shows that the predictions by both the Nakayama et al. model and the present model are comparable. Nakayama et al. [21] model matches well with their own experimental results whereas the prediction of Chein and Webb data [22] by the present model appears better. Chein and Webb model grossly under predicts both the sets.

6. Conclusions

A methodology for the prediction of boiling heat flux and bubble frequency from a tunnel and pore micro-structure has been discussed in this article. Based on the assumption of the suction evaporation mode the present model judiciously uses the features of both the Nakayama et al. [21] model and Chein and Webb [22] model. The present model needs three empirical constant compared to seven by Nakayama et al. [21] and two by Chein and Webb [22].

A thorough analysis has been carried out for the liquid refill stage ignored in all the previous models. The mechanistic model of liquid intake developed in the present work shows the intake time to be small compared to the duration of the other two phases at large pool height. However, the intake time could be significant for smaller pool height and depressurized systems. The prediction of the model shows a good agreement with the experimental data in the literature.

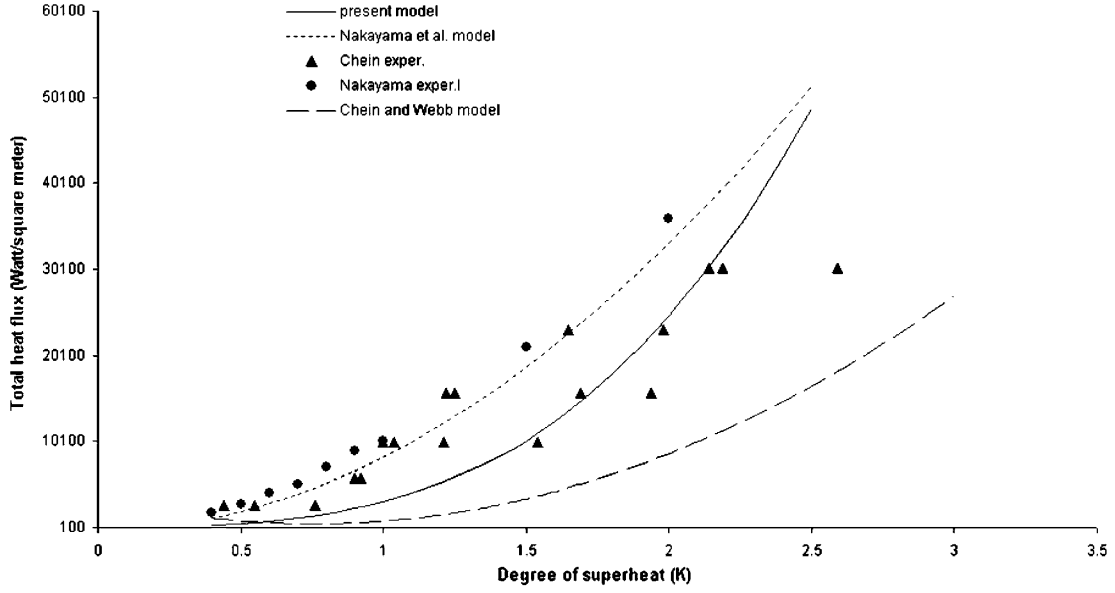

Fig. 9. Prediction of heat flux in proposed model and comparison with previous models at a pool height of 0.15 m.

Acknowledgement

The financial support extended by M.H.R.D., India towards the project is gratefully acknowledged.

References

[1] M. Jacob, Heat Transfer, Wiley, New York, 1949, pp. 636–638.
[2] A.E. Bergles, Enhancement of pool boiling, Int. J. Refrig. 20 (8) (1997) 545–551.
[3] D.B.R. Kenning, New developments in pool boiling, Int. J. Refrig. 20 (8) (1997) 534–543.
[4] R.L. Webb, The evolution of enhanced surface geometries for nucleate boiling, Heat Transfer Eng. 2 (1981) 46–69.
[5] R.L. Webb, Odyssey of the enhanced boiling surface, ASME J. Heat Transfer 126 (6) (2004) 1051–1059.
[6] D.F. Chao, N. Zhang, W.J. Yang, Nucleate pool boiling on copper–graphite composite surfaces and its enhance mechanism, J. Thermophys. Heat Transfer 18 (2) (2004) 236–242.
[7] G.W. Yang, W. Yang, N. Zhang, Mechanisms of nucleate pool boiling on composite surfaces, Int. Commun. Heat Mass Transfer 19 (6) (1992) 781–790.
[8] J.H. Kim, K.N. Rainey, S.M. You, J.Y. Pak, Mechanism of nucleate boiling heat transfer enhancement from microporous surface in saturated FC 72, Trans. ASME J. Heat Transfer 124 (2002) 501–506.
[9] J.Y. Chang, S.M. You, Boiling heat transfer phenomena from microporous and porous surfaces in saturated FC-72, Int. J. Heat Mass Transfer 40 (18) (1997) 4437–4447.
[10] Y. Fujita, S. Uchida, Enhanced nucleate boiling heat transfer in a narrow confined space between a heating surface and a slitted plate, J. Enhanced Heat Transfer 2 (1–2) (1995) 105–114.
[11] Y. Zhao, T. Tsuruta, C. Ji, Experimental study of nucleate boiling heat transfer enhancement in confined space, Exp. Thermal Fluid Sci. 28 (2003) 9–16.
[12] H.M. Chou, R.F. Horng, Y.S. Liu, J.L. Wong, The effect of grooved pattern on enhanced boiling heat transfer in a cylindrical tank base with a constant surface area, Int. Commun. Heat Mass Transfer 29 (7) (2002) 951–960.
[13] P. Griffith, J.D. Wallis, The role of surface condition in nucleate boiling, Chem. Eng. Prog. Symp. Ser. 55 (1959) 49–63.
[14] J. Arshad, J.R. Thome, Enhanced boiling surfaces: heat transfer mechanism mixture boiling, Proc. ASME–JSME Therm. Eng. Joint Conf. 1 (1983) 191–197.
[15] W. Nakayama, T. Daikoku, H. Kuwahara, T. Nakajima, Dynamic model of enhanced boiling heat transfer on porous surfaces – Part I. Experimental investigation, ASME J. Heat Transfer 102 (3) (1980) 445–450.
[16] M.D. Xin, Y.D. Chao, Analysis and experiment of boiling heat transfer on T-shaped finned surfaces, in: National Heat Transfer Conference, 1985.
[17] K.G. Rajalu, R. Kumar, B. Mohanty, H.K. Varma, Enhancement of nucleate pool boiling heat transfer coefficient by reentrant cavity surfaces, Heat Mass Transfer 41 (2) (2004) 127–132.
[18] I.L. Pioro, W. Rohsenow, S.S. Doerffer, Nucleate pool-boiling heat transfer, I: review of parametric effects of boiling surfaces, Int. J. Heat Mass Transfer 41 (14) (1998) 2183–2195.
[19] L.H. Chein, R.L. Webb, Parametric studies of nucleate pool boiling on structured surfaces, part I: effect of tunnel dimension, ASME J. Heat Transfer 120 (1998) 1042–1048.
[20] Y.Y. Hsu, R.W. Graham, An analytical and experimental study of the thermal boundary layer and ebullition cycle in nucleate boiling, NASA TN D-594, 1961.
[21] W. Nakayama, T. Daikoku, H. Kuwahara, T. Nakajima, Dynamic model of enhanced boiling heat transfer on porous surfaces – part II: analytical model, ASME J. Heat Transfer 102 (3) (1980) 451–456.
[22] L.H. Chein, R.L. Webb, A nucleate boiling model for structured enhanced surfaces, Int. J. Heat Mass Transfer 41 (14) (1998) 2183–2195.
[23] C. Ramaswamy, Y. Joshi, W. Nakayama, W. Johnson, Semi-analytical model for boiling from enhanced surface, Int. J. Heat Mass Transfer 46 (2003) 4257–4269.
[24] Y.Y. Jiang, W.C. Wang, D. Wang, B.X. Wang, Boiling heat transfer on machined porous surfaces with structural optimization, Int. J. Heat Mass Transfer 44 (2001) 443–456.
[25] D. Khrustalev, A. Faghri, Thermal analysis of a micro heat pipe, J. Heat Transfer 116 (1994) 189–198.
[26] B.B. Mikic, W.M. Rohsenow, Bubble growth rates in non-uniform temperature field, Prog. Heat Mass Transfer 2 (1969) 283–292.
[27] I. Haider, A theoretical and experimental study of nucleate pool boiling enhancement of structured surfaces, Ph.D. Thesis, Penn State University, PA, USA, 1994.
[28] B.B. Mikic, W.M. Rohsenow, A new correlation of pool-boiling data including the effect of heating surfaces, J. Heat Transfer 91 (1969) 245–250.
[29] A.A.K. Tehrani, M.A. Patrick, A.A. Wragg, Dynamic fluid flow behavior of a tank draining through a vertical tube, Int. J. Multiphase Flow 18 (1992) 977–988.
[30] G.B. Wallis, One-Dimensional Two-Phase Flow, McGraw-Hill, New York, 1969.